VERSITA

DOI: 10.2478/s11696-007-0007-6

Thermodynamic Possibilities and Constraints of Pure Hydrogen Production by a Chromium, Nickel, and Manganese-Based Chemical Looping Process at Lower Temperatures

[a,b]K. SVOBODA, [a]A. SIEWIOREK, [a]D. BAXTER, [a,c]J. ROGUT, and [b]M. PUNČOCHÁŘ

[a] *Institute for Energy, Joint Research Centre of EC, 1755 ZG Petten, The Netherlands*
e-mail: karel.svoboda@jrc.nl, aleksandra.siewiorek@jrc.nl, david.baxter@jrc.nl

[b] *Institute of Chemical Process Fundamentals, Academy of Sciences of the Czech Republic, Rozvojová 135, 165 02 Prague, Czech Republic*
e-mail: svoboda@icpf.cas.cz

[c] *Central Mining Institute, Plac Gwarkow 1, 40 166 Katowice, Poland*
e-mail: rogutjan@yahoo.com

Received 25 August 2006; Revised 3 October 2006; Accepted 2 November 2006

The reduction of chromium, nickel, and manganese oxides by hydrogen, CO, CH_4, and model syngas (mixtures of CO + H_2 or H_2 + CO + CO_2) and oxidation by water vapor has been studied from the thermodynamic and chemical equilibrium point of view. Attention was concentrated not only on the convenient conditions for reduction of the relevant oxides to metals or lower oxides at temperatures in the range 400—1000 K, but also on the possible formation of soot, carbides, and carbonates as precursors for the carbon monoxide and carbon dioxide formation in the steam oxidation step. Reduction of very stable Cr_2O_3 to metallic Cr by hydrogen or CO at temperatures of 400—1000 K is thermodynamically excluded. Reduction of nickel oxide (NiO) and manganese oxide (Mn_3O_4) by hydrogen or CO at such temperatures is feasible. The oxidation of MnO and Ni by steam and simultaneous production of hydrogen at temperatures between 400 and 1000 K is a difficult step from the thermodynamics viewpoint. Assuming the Ni—NiO system, the formation of nickel aluminum spinel could be used to increase the equilibrium hydrogen yield, thus, enabling the hydrogen production *via* looping redox process. The equilibrium hydrogen yield under the conditions of steam oxidation of the Ni—NiO system is, however, substantially lower than that for the Fe—Fe_3O_4 system. The system comprising nickel ferrite seems to be unsuitable for cyclic redox processes. Under strongly reducing conditions, at high CO concentrations/partial pressures, formation of nickel carbide (Ni_3C) is thermodynamically favored. Pressurized conditions during the reduction step with CO/CO_2 containing gases enhance the formation of soot and carbon-containing compounds such as carbides and/or carbonates.

Keywords: hydrogen, chromium, nickel, manganese, chemical looping, thermodynamics

INTRODUCTION

Hydrogen is expected to become an important energy carrier for sustainable energy production, transformation, and consumption with reduced impact on the local and global environment. The development of hydrogen-based energy and transport systems needs reliable and inexpensive methods of relatively pure hydrogen production, storage, and supply.

Already at the beginning of the last century, the knowledge and experience from iron metal production by redox process was used to convert steam into hydrogen in a high-temperature iron-based cyclic process [1]. This process was applied to produce large quantities of hydrogen. Renewed interest in this so-called sponge iron reaction was recently reported [2—4], proposing even the conversion of hydrocarbons and synthesis gas produced from solid biomass into fuel cell-grade hydrogen [4].

The two-step water splitting processes based on

redox reactions have been previously studied theoretically [5] and experimentally at higher temperatures [6]. Typically a transitional metal or reduced form of the metal oxides (*e.g.* Fe, Ni, Ce_2O_3) were oxidized by water vapor at temperatures over 400 ℃ and then reduced *via* thermal decomposition in an inert gas at temperatures exceeding 1000 ℃. The thermal energy consumed during the reduction step was supplied by concentrated solar or simulated solar energy.

Investigation of metallic oxides for chemical looping combustion of gaseous and solid fuels with the aim to produce a stream of concentrated CO_2 [7—10], contributed to better knowledge of the properties and behavior of various metal—metal oxide systems *via* the cyclic oxidation by oxygen and reduction by various carbon-containing fuels.

Iron, as a common metal, has been suggested for hydrogen production by reaction with steam at temperatures higher than 750 ℃ [3]. The basic principle of the cyclic iron sponge process is the iron oxides reduction using reducing gases (H_2, CO, CH_4, *etc.*) and then the iron oxidation by steam to produce hydrogen. In this redox process a syngas (*e.g.* from biomass gasification [4]) or a gas mixture from steam reforming of hydrocarbon fuels can be converted into relatively pure hydrogen [11].

The redox cycles at relatively high working temperatures (over 750 ℃) frequently cause structural changes, agglomeration, sintering, and deactivation of iron and similar metals. For this reason an attempt has been done to explore the possibility of a cyclic process for clean hydrogen production/storage at lower temperatures (below 700 ℃). High reactivity of solid reactants at lower temperatures commonly requires highly reactive, large surface (or a high dispersion) of a metal/metal oxide, catalysts, a convenient support/carrier, and the addition of stable compounds for changing redox conditions [12—15].

Another disadvantage of the use of iron in the redox cyclic process of hydrogen production is the possibility of soot and Fe_3C formation during iron reduction by CO- and CO_2-containing gases [16]. Then, during the steam oxidation of sponge iron, the presence of carbon and iron carbide caused that hydrogen was produced together with carbon-containing impurities.

Relatively cheap and common alloying elements Cr, Ni, and Mn have been chosen for the basic thermodynamic study for the cyclic hydrogen production at relatively lower temperatures with respect to iron. The reduction of chromium, nickel, and manganese oxides by hydrogen, CO, CH_4, and model syngas (mixtures of H_2 + CO + CO_2) as well as oxidation of the corresponding metals by water vapor has been studied from the thermodynamics and chemical equilibrium point of view. Attention has been concentrated not only on the convenient conditions for reduction of the relevant oxides to metals or lower oxides at temperatures in the range 400—1000 K, but also on the possible formation of undesired soot, carbides, and carbonates as precursors for carbon monoxide and carbon dioxide formation during the steam oxidation step.

THEORETICAL

Gibbs energy for individual reactions, ΔG_r, has been computed according to the general scheme

$$\Delta G_r = \sum_i \nu_i (\Delta G_f)_i \qquad (1)$$

where ν_i and $(\Delta G_f)_i$ (positive for products and negative for input reactants) represent the stoichiometric coefficient and Gibbs energy of formation of the component i participating in the chemical reaction, respectively.

Based on the value of ΔG_r, chemical reactions could be classified as reversible with ΔG_r value ranging within approximately -25 kJ mol^{-1} and $+25$ kJ mol^{-1}, reactions tending strongly towards the reaction products $\Delta G_r < -25$ kJ mol^{-1}, and those presenting almost negligible conversion $\Delta G_r > 25$ kJ mol^{-1}.

For the promising or important reactions, from the point of view of the cyclic hydrogen production, reaction enthalpies have been computed according to the general scheme

$$\Delta H_r = \sum_i \nu_i (\Delta H_f)_i \qquad (2)$$

where $(\Delta H_f)_i$ denotes the enthalpy of formation of the component i participating in the chemical reaction.

The chemical equilibrium for a general reaction considering solid (s) and gaseous (g) reactants and products

$$\nu_A\,A_s + \nu_B\,B_g + \nu_C\,C_g \longleftrightarrow \nu_D\,D_s + \nu_E\,E_g + \nu_F\,F_g \quad (A)$$

is characterized by the equilibrium constant, K_r, expressed as

$$K_r = \frac{[D_s]^{\nu_D}[E_g]^{\nu_E}[F_g]^{\nu_F}}{[A_s]^{\nu_A}[B_g]^{\nu_B}[C_g]^{\nu_C}} \qquad (3)$$

where the terms $[D_s]$, $[E_g]$, and $[F_g]$ denote activities of solid and gaseous products and the terms $[A_s]$, $[B_g]$, and $[C_g]$ represent activities of the input solid and gaseous components.

Activity of solid compounds under common conditions (non-reactive toward other solid phases) was taken as equal to 1. Activity of gaseous species at lower pressures and higher temperatures (far from their critical points) was taken as identical with partial pressure of the corresponding gaseous species. As the component partial pressure could be expressed by means of the total (system) pressure P_{tot} and the mole fraction x of the gaseous species, eqn (*3*) could be rewritten as

$$K_r = P_{tot}^{\sum_i \nu_i} \prod_i x_i^{\nu_i} \qquad i = \text{B, C, E, F} \qquad (4)$$

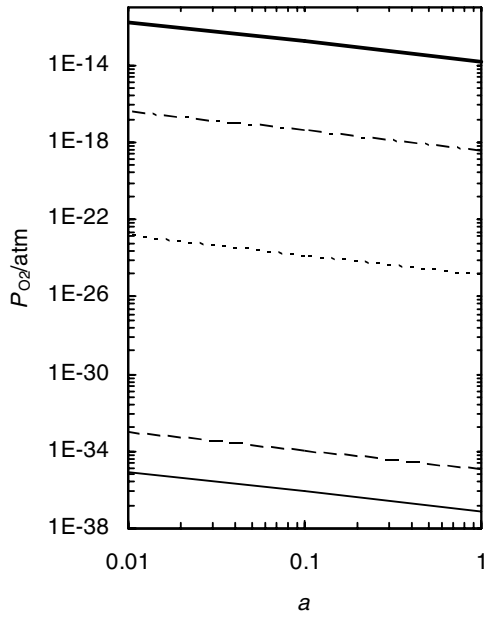

Fig. 1. Variation of the equilibrium partial pressure of oxygen with the activity of reduced form of the selected redox systems at 900 K. Mn—MnO (solid line), Cr—Cr_2O_3 (dashed line), Fe—FeO (dotted line), Ni—NiO (dotted-dashed line), and MnO—Mn_3O_4 (thick solid line).

The reaction constant K_r is related with the reaction Gibbs energy *via* the following expression

$$K_r = \exp\left(-\Delta G_r/RT\right) \qquad (5)$$

where T is the absolute temperature and R denotes the universal gas constant.

Cyclic processes for repeated reduction of metal oxides (*e.g.* by syngas or methane) and oxidation of the metal (lower oxide) by steam require "reasonable reaction ability" for transition of metal to metal oxide and *vice versa*. The equilibrium pressures of oxygen for the oxidation of Cr to Cr_2O_3, Mn to MnO, Fe to FeO, Ni to NiO, and MnO to Mn_3O_4 at 900 K are compared in Fig. 1. Activity of a metal and the corresponding metal oxides affects the value of equilibrium P_{O_2}. Lower metal activity and higher activity of the metal oxides formed generally increases the equilibrium partial pressure of oxygen, thus, obstructing the metal oxidation (Fig. 1). Lower activity of the oxidized form (*e.g.* as a consequence of consecutive chemical reaction of the metal oxide) shifts the reaction equilibrium towards the oxide formation, *i.e.* the equilibrium P_{O_2} decreases.

Metals requiring low oxygen partial pressures to start their oxidation, for example chromium and manganese, are oxidized very easily, but, the reduction of their oxides can be expected to be very difficult. On the other hand, if a relatively high oxygen partial pressure is necessary for starting the oxidation of metals or lower metallic oxides, such as Cu, Ni, or MnO, oxidation of the corresponding metal or metal oxide by steam can be considered as problematic. On the other hand, the reverse reaction is likely to proceed, *i.e.* the resulting oxides can act as oxidants.

The most convenient metal—metal oxide system for the cyclic redox process of hydrogen production/storage should be somewhere between the abovementioned two extreme cases, *e.g.* near the line calculated for the Fe—FeO redox system in Fig. 1.

RESULTS

Reactions with Chromium Compounds

For chromium Cr_2O_3, CrO_2, and CrO_3 were considered. Thermodynamic properties of CrO_2 (solid) and CrO_3 are given in the relevant literature [17] only for the temperatures lower than 600 K.

The reaction enthalpy and reaction Gibbs energy have been computed from tabulated data of formation enthalpies of compounds and Gibbs energies of formation [17]. Three basic reduction reactions of chromium oxides were taken into account, *e.g.* the reaction with hydrogen, CO, and CH_4. The reaction Gibbs energy calculated for the reactions of Cr_2O_3 in the temperature range 400—1000 K is given in Table 1.

The following reactions have been thermodynamically analyzed

$$Cr_2O_3(s) + 3H_2(g) \longleftrightarrow 2Cr(s) + 3H_2O(g) \qquad (B)$$

$$Cr_2O_3(s) + 3CO(g) \longleftrightarrow 2Cr(s) + 3CO_2(g) \qquad (C)$$

$$Cr_2O_3(s) + 3/4CH_4(g) \longleftrightarrow 2Cr(s) + 3/4CO_2(g) + 3/2H_2O(g) \qquad (D)$$

Based on the data given in Table 1 one can conclude that the reduction of Cr_2O_3 to metallic Cr is thermodynamically excluded in the chosen temperature range. The reaction enthalpy ΔH_r for the reactions (B) and (C) is approximately in the range of 280—410 kJ mol^{-1} and for the reaction (D) it is over 500 kJ mol^{-1}, *i.e.* Cr_2O_3 is very stable in the relevant temperature range. Thermodynamic analysis of Cr_2O_3 oxidation to CrO_2 and CrO_3 by H_2O and CO_2 is given in Table 2. Assuming the reactions

$$Cr_2O_3(s) + H_2O(g) \longleftrightarrow 2CrO_2(s) + H_2(g) \qquad (E)$$

Table 1. Reaction Gibbs Energy for the Reactions of Cr_2O_3

T/K	ΔG_r/(kJ mol^{-1})		
	(B)	(C)	(D)
400	358.8	285.8	430.2
600	336.0	286.3	378.0
800	316.1	287.8	326.6
1000	298.1	289.6	275.9

Table 2. Reaction Gibbs Energy for Cr_2O_3 and CrO_2 Oxidation by H_2O and CO_2

T/K	ΔG_r/(kJ mol^{-1})			
	(E)	(F)	(G)	(H)
400	199.5	223.9	265.1	289.5
500	200.1	220.4	269.0	289.4
600	198.9	215.5	270.6	287.2

Table 3. Reaction Gibbs Energy for the Reactions of NiO with H_2, CO, and CH_4

T/K	ΔG_r/(kJ mol^{-1})			
	(I)	(J)	(K)	(L)
400	−21.95	−46.29	53.77	7.48
600	−30.11	−46.68	−17.90	−64.58
800	−37.12	−46.56	−88.21	−134.78
1000	−43.48	−46.31	−157.55	−203.86

$$Cr_2O_3(s) + CO_2(g) \longleftrightarrow 2CrO_2(s) + CO(g) \qquad (F)$$

$$CrO_2(s) + H_2O(g) \longleftrightarrow CrO_3(s) + H_2(g) \qquad (G)$$

$$CrO_2(s) + CO_2(g) \longleftrightarrow CrO_3(s) + CO(g) \qquad (H)$$

the Gibbs energy of formation of CrO_2 and CrO_3 is unfortunately available only up to the maximum temperature of 600 K [17].

Again, it can be concluded that the oxidation of Cr_2O_3 and CrO_2 by steam and CO_2 is thermodynamically excluded at lower temperatures. Dichromium trioxide is a very stable compound with respect to both oxidation and reduction. CrO_2 can only be easily reduced to Cr_2O_3, the reverse oxidation by steam or CO_2 is thermodynamically impossible. Thus, the systems comprising chromium oxides should be considered as inconvenient for the cyclic redox processes of hydrogen production at temperatures below 1000 K. The stability and resistance to carburization of Cr_2O_3 under strongly reducing conditions could be utilized in carrier materials for the reacting species (Me—MeO) in the redox reactions.

Reactions with Nickel Compounds and Alloys

In the case of nickel the only stable oxide compound (NiO) has been considered [9, 17, 18]. Moreover, thermodynamic capability of nickel ferrite ($NiFe_2O_4$) and nickel aluminum spinel ($NiAl_2O_4$) for the cyclic redox reactions has also been analyzed.

The reaction Gibbs energy for the reactions of pure NiO with reducing species

$$NiO(s) + H_2(g) \longleftrightarrow Ni(s) + H_2O(g) \qquad (I)$$

$$NiO(s) + CO(g) \longleftrightarrow Ni(s) + CO_2(g) \qquad (J)$$

$$3NiO(s) + CH_4(g) \longleftrightarrow 3Ni(s) + 2H_2O(g) + CO(g) \qquad (K)$$

$$4NiO(s) + CH_4(g) \longleftrightarrow 4Ni(s) + 2H_2O(g) + CO_2(g) \qquad (L)$$

in the temperature range of 400—1000 K is given in Table 3. At given conditions, the reaction enthalpies ΔH_r for the reactions (I) and (J) are approximately in the range of −3.7 kJ mol^{-1} to −12.9 kJ mol^{-1} and −44.3 kJ mol^{-1} to −47.7 kJ mol^{-1}, respectively. The reactions of NiO with CH_4 are strongly endothermic, the values of ΔH_r for the reaction (L) are approximately in the range of 139—155 kJ mol^{-1}.

Taking into account the data given in Table 3, NiO is relatively easily reduced to metallic Ni. On the other hand, at lower temperatures steam conversion to hydrogen by Ni is lower than 1 %.

The equilibrium hydrogen concentration calculated for the reverse reaction (I) is low, however, if the NiO activity is reduced, *e.g.* by its reactions with some other solid material or carrier, the yield of hydrogen could be increased. Two examples of such reactions are analyzed below, *i.e.* formation of nickel ferrite [19, 20] and spinel $NiO \cdot Al_2O_3$ [21—23].

Homogeneous reactive nickel ferrite $NiFe_2O_4$ can be obtained *e.g.* by controlled thermal decomposition of Ni^{II} and Fe^{III} formate [19] (and similar salts) or by coprecipitation followed by hydrothermal treatment [20].

Equilibrium data (ΔG_r) for the reduction of nickel ferrite to iron and nickel by hydrogen, CO, and methane according to the reactions (M)—(O) are collected in Table 4 showing that the reduction of nickel ferrite by CO is thermodynamically possible over a broad range of temperatures. Reduction of $NiFe_2O_4$ by methane is feasible only at higher temperatures (over 800 K).

$$1/4NiFe_2O_4(s) + H_2(g) \longleftrightarrow 1/4Ni(s) + 1/2Fe(s) + H_2O(g) \qquad (M)$$

$$1/4NiFe_2O_4(s) + CO(g) \longleftrightarrow 1/4Ni(s) + 1/2Fe(s) + CO_2(g) \qquad (N)$$

$$NiFe_2O_4(s) + CH_4(g) \longleftrightarrow Ni(s) + 2Fe(s) + 2H_2O(g) + CO_2(g) \qquad (O)$$

The reaction enthalpies ΔH_r for the reactions (M) and (N) carried out in the temperature range of 400—1000 K are approximately in the range of 27 kJ mol^{-1} to 18.7 kJ mol^{-1} and −13.5 kJ mol^{-1} to −16.1 kJ mol^{-1}, respectively. The reduction of $NiFe_2O_4$ by CH_4 is a strongly endothermic reaction with ΔH_r approximately in the range of 278—266 kJ mol^{-1}.

Table 4. Reaction Gibbs Energy for the Reduction Reactions of $NiFe_2O_4$

T/K	ΔG_r/(kJ mol^{-1})		
	(M)	(N)	(O)
400	10.084	−14.257	135.63
600	2.225	−14.339	64.77
800	−4.673	−14.111	−4.97
1000	−10.836	−13.672	−73.30

Table 5. Equilibrium Gas Phase Content of H_2 for the Reactions (I) and (M), CO for the Reaction (N), and CH_4 for the Reaction (O)

T/K	x_{H_2}/vol. %		x_{CO}/vol. %	x_{CH_4}/vol. %
	(I)	(M)	(N)	(O)
400	0.134	95.42	1.35	99.999
600	0.236	60.99	5.32	97.54
800	0.372	33.1	10.67	5.85
1000	0.528	21.32	16.15	0.002

Table 6. Reaction Gibbs Energy for the Reactions of Steam Oxidation of Ni + Fe and Fe

T/K	ΔG_r/(kJ mol^{-1})		
	(P)	(Q)	(R)
400	−40.336	−34.423	−56.376
600	−8.899	−8.601	−38.715
800	18.693	12.229	−24.895
1000	43.343	29.256	−14.221

Table 7. Reaction Gibbs Energy for the Formation of $NiAl_2O_4$ and Reactions of γ-Al_2O_3 with Water Vapor

T/K	ΔG_r/(kJ mol^{-1})	
	(S)	(T)
400	−22.58	−24.40
500	−23.34	−10.13
600	−23.85	∼4.5
800	−24.49	
1000	−24.83	

The equilibrium concentrations of H_2, CO, and CH_4 for the corresponding reactions and comparison with equilibrium H_2 concentrations for the reaction (I) are given in Table 5.

Oxidation of a mixture of nickel and iron (resulting from the $NiFe_2O_4$ reduction) by steam at lower temperatures is, however, complicated. Three possible oxidation routes (reactions (P)—(R)) are thermodynamically analyzed in terms of ΔG_r in Table 6.

$$\mathrm{Ni(s) + 2Fe(s) + 4H_2O(g) \longleftrightarrow NiFe_2O_4(s) + 4H_2(g)} \qquad (P)$$

$$\mathrm{Ni(s) + 2Fe(s) + 11/3H_2O(g) \longleftrightarrow NiO(s) + 2/3Fe_3O_4(s) + 11/3H_2(g)} \qquad (Q)$$

$$\mathrm{2Fe(s) + 8/3H_2O(g) \longleftrightarrow 2/3Fe_3O_4(s) + 8/3H_2(g)} \qquad (R)$$

The resulting ΔG_r data in Table 6 suggest that the reaction (R) with no oxidation of Ni is the most probable one from the theoretical point of view, *i.e.* the simultaneous oxidation of the Fe—Ni mixture to form nickel ferrite by steam is significantly less probable. Thus, as iron is substantially more reactive in steam oxidation than nickel, practical exploitation of the nickel ferrite in redox cycles for hydrogen production is restricted or impossible.

Another enhanced hydrogen production using Ni oxidation by water vapor is carried out in the presence of reactive γ-alumina. At given reaction conditions oxidized form of nickel, NiO, reacts in the solid phase with alumina to give the nickel—aluminum spinel

$$\mathrm{NiO(s) + \gamma\text{-}Al_2O_3(s) \longleftrightarrow NiAl_2O_4(s)} \qquad (S)$$

At lower temperatures γ-Al_2O_3 tends to react with water vapor forming boehmite

$$\mathrm{\gamma\text{-}Al_2O_3(s) + H_2O(g) \longleftrightarrow Al_2O_3 \cdot H_2O(s)} \qquad (T)$$

while at temperatures exceeding approximately 600 K the reaction (S) is favored. Reaction Gibbs energy of the reactions (S) and (T) is shown in Table 7.

Therefore, at temperatures higher than 600 K the oxidation of Ni with steam and γ-Al_2O_3 is thermodynamically possible

$$\mathrm{Ni(s) + \gamma\text{-}Al_2O_3(s) + H_2O(g) \longleftrightarrow NiAl_2O_4(s) + H_2(g)} \qquad (U)$$

In fact, the reaction rate will be strongly dependent on the intimacy of both solids and a magnitude of the specific surface area. In Table 8, the values of ΔG_r, K_r, and hydrogen concentrations at equilibrium conditions are compared for this reaction and that of steam oxidation of metallic Ni (reverse reaction (I))

$$\mathrm{Ni(s) + H_2O(g) \longleftrightarrow NiO(s) + H_2(g)} \qquad (V)$$

Presented data show that the attainable equilibrium concentration of hydrogen is, for the case of NiO—alumina spinel formation, 1 to 2 orders of magnitude higher than those calculated for the case of Ni

Table 8. Comparison of ΔG_r, K_r, and Hydrogen Content in the Gas Phase at Equilibrium Conditions for the Reactions of Ni Oxidation by Water Vapor

T/K	ΔG_r/kJ mol^{-1})		K_r		x_{H_2}/vol. %	
	(*U*)	(*V*)	(*U*)	(*V*)	(*U*)	(*V*)
600	6.266	30.114	0.28416	0.002365	22.13	0.236
800	12.633	37.124	0.14919	0.003731	12.98	0.372
1000	18.651	43.477	0.10570	0.005310	9.56	0.528

oxidation to NiO with steam. The equilibrium hydrogen volumetric concentrations are still, even for the reaction (*U*), lower in comparison with steam oxidation of iron, for which the equilibrium steam conversion at temperatures lower than 800 K is higher than 80 % [24].

Reduction of nickel—aluminum spinel is more difficult than the reduction of NiO, *i.e.* during simultaneous reduction of NiO and $NiAl_2O_4$ the nickel oxide will be reduced preferably [23, 25, 26]. On the other hand, the dispersion of nickel is higher after the reduction of $NiAl_2O_4$ in comparison with the reduction of NiO prepared by simple impregnation of alumina [26]. The temperature for the Ni—Al spinel formation should be relatively low [22], annealing time relatively short, and the surface area available for the reaction as large as possible. Otherwise, it was found that the reduction of the $NiAl_2O_4$ spinel under the conditions of chemical looping combustion at temperatures exceeding 800 ℃ was difficult to carry out [23, 26]. Thus, repeated formation and decomposition of the nickel—aluminum spinel (without formation of separate phases) at temperatures between 600 K and 1000 K is a crucial prerequisite for the successful application of such system for cyclic hydrogen production.

The equilibrium gas composition for hydrogen and CO reduction of NiO, $NiFe_2O_4$, and $NiAl_2O_4$ is independent on the operating pressure or the presence of inert gaseous species. However, the reduction of NiO by methane, (reactions (*K*) and (*L*)), depends on these variables. Decreasing the operating pressure and increasing the amount of inert gas will improve the conversion of NiO and CH_4.

During the reduction of NiO with CO and CH_4, the carbon formation, deposition, and nickel carbide formation is thermodynamically possible

$$3Ni(s) + 2CO(g) \longleftrightarrow Ni_3C(s) + CO_2(g) \qquad (W)$$

$$3Ni(s) + CH_4(g) \longleftrightarrow Ni_3C(s) + 2H_2(g) \qquad (X)$$

The corresponding values of ΔG_r for the two reactions between 400 K and 800 K [17] are summarized in Table 9. The formation of Ni_3C is thermodynamically favored at higher CO and lower water vapor content in the reducing gas. Higher operating pressure will cause higher conversions of nickel to Ni_3C according to the reaction (*W*). Nickel carbide formation is, however, rather improbable or even excluded in the case of the reaction of Ni with methane at temperatures between 400 K and 800 K.

Table 9. Reaction Gibbs Energy and Equilibrium Constant for the Formation of Ni_3C

T/K	ΔG_r/kJ mol^{-1})		K_r
	(*W*)	(*X*)	(*W*)
400	−39.167	104.771	132891.6
600	−6.77	82.381	3.894
800	25.53	58.369	0.02139

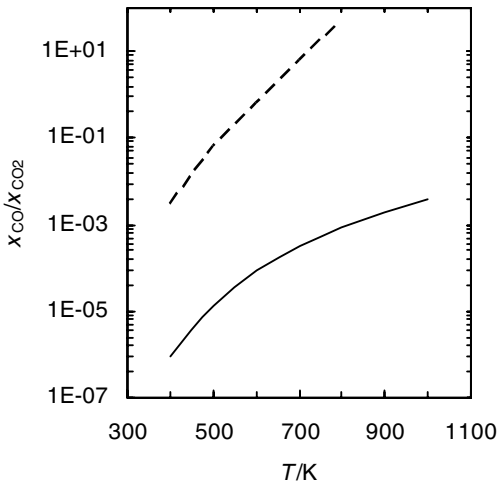

Fig. 2. Comparison of the equilibrium CO to CO_2 mole (volumetric) ratio for the reactions (*J*) (solid line) and (*W*) (dashed line).

Comparison of equilibrium mole (or volumetric) ratio of CO/CO_2 for the reactions (*J*) and (*W*), *i.e.* for the reduction of NiO by CO and the formation of Ni_3C in a consecutive reaction of Ni with CO is given in Fig. 2 for the operating pressure of 1 atm. It was found that the equilibrium CO to CO_2 mole ratio for the reduction of NiO to Ni is substantially lower than that for the formation of nickel carbide Ni_3C from Ni. Nevertheless, the formation of Ni_3C cannot be excluded, particularly at temperatures below 700 K and under elevated pressure.

Table 10. Reaction Gibbs Energy for the Formation of $NiCO_3$

T/K	ΔG_r/(kJ mol^{-1})		
	(Y)	(Z)	(AA)
400	4.82	51.11	26.77
500	21.23	67.86	47.5
600	37.68	84.36	67.80
700	54.04	100.68	87.76

Table 11. Reaction Gibbs Energy for the Decomposition of $NiCO_3$ and Ni_3C

T/K	ΔG_r/(kJ mol^{-1})		
	(Y)	(AB)	(AC)
400	−4.82	80.69	56.34
500	−21.23	81.39	61.02
600	−37.68	80.55	63.98
700	−54.04	78.79	65.86
800		76.40	66.97

At rather lower temperature (below 700 K [17]) and higher CO_2 partial pressure, also $NiCO_3$ formation is thermodynamically allowed

$$NiO(s) + CO_2(g) \longleftrightarrow NiCO_3(s) \qquad (Y)$$

$$Ni(s) + 2CO_2(g) \longleftrightarrow NiCO_3(s) + CO(g) \qquad (Z)$$

$$Ni(s) + CO_2(g) + H_2O(g) \longleftrightarrow NiCO_3(s) + H_2(g) (AA)$$

In the temperature range of 400—700 K the reaction enthalpy, ΔH_r, for the reactions (Y)—(AA) is approximately −60 kJ mol^{-1} to −61 kJ mol^{-1}, −12.9 kJ mol^{-1} to −16.5 kJ mol^{-1}, and −51 kJ mol^{-1} to −57 kJ mol^{-1}, respectively. The corresponding values of ΔG_r for the $NiCO_3$ formation are given in Table 10. It can be seen that at temperatures over 600 K the formation of $NiCO_3$ is rather improbable at lower operating pressures. The reaction (Z) is almost excluded from the viewpoint of thermodynamics. In the presence of reactive γ-alumina and at temperatures higher than 600 K NiO reacts preferentially with alumina than with CO_2.

Simultaneously with Ni, also nickel carbide Ni_3C (formed by the reactions (W) and (X)) is oxidized by steam

$$Ni_3C(s) + 4H_2O(g) \longleftrightarrow 3NiO(s) + CO(g) + 4H_2(g) \qquad (AB)$$

$$Ni_3C(s) + 5H_2O(g) \longleftrightarrow 3NiO(s) + CO_2(g) + 5H_2(g) \qquad (AC)$$

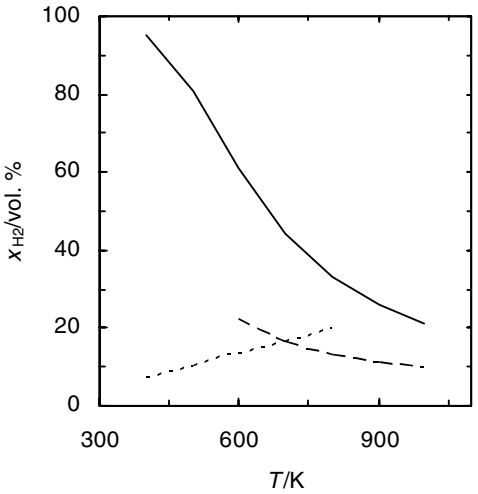

Fig. 3. Equilibrium concentrations of hydrogen in the gas phase for the reverse reaction (M) (solid line) and the reactions (U) (dashed line) and (AC) (dotted line).

and $NiCO_3$ is decomposed into NiO and CO_2 *via* the reverse reaction (Y). The reactions are thermodynamically more probable than the reactions of Ni oxidation with steam, particularly the decomposition of $NiCO_3$ and decomposition of nickel carbide according to reaction (AC). Therefore, the produced hydrogen could be contaminated by CO_2 and CO. The ΔG_r values for the reactions (AB), (AC), and the reverse equation (Y) are summarized in Table 11.

To compare the ΔG_r values with those for Ni oxidation by steam stoichiometry of the corresponding reactions should be taken into account. In the presence of active γ-Al_2O_3 the corresponding ΔG_r values will be more negative and the equilibrium constants will be higher.

Fig. 3 shows the comparison of the equilibrium hydrogen mole fraction in the gas phase for the steam oxidation of Ni and Fe (reverse reaction (M)), Ni with alumina and H_2O (reaction (U)), and the reaction of Ni_3C with H_2O (AC). Fig. 4 illustrates the equilibrium mole fraction of CO and CO_2 in the gas phase in the temperature range of 400—800 K for the reactions (AB) and (AC).

Reactions with Manganese Compounds

For manganese oxides, four relevant oxides, MnO, Mn_3O_4, Mn_2O_3, and MnO_2 have been checked [17] for the redox cycling reactions.

Previously, the three basic manganese oxides have been analyzed for redox processes and hydrogen production from steam [27]. MnO is very stable oxide, resistant to reduction and forming slightly nonstoichiometric higher oxides [28]. In many aspects MnO behaves rather like a metal (*e.g.* see Fig. 1). The reduction of MnO to metallic Mn by hydrogen or CO is thermodynamically excluded at temperatures

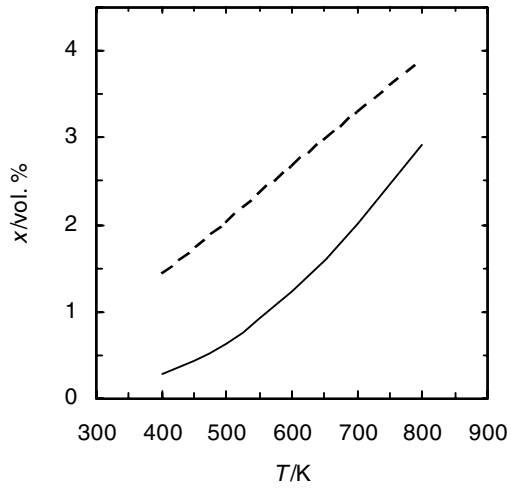

Fig. 4. Equilibrium concentrations of CO and CO_2 formed during the reactions (AB) (solid line) and (AC) (dashed line), respectively.

Table 12. Reaction Gibbs Energy for the Mn_3O_4 Reduction

T/K	ΔG_r/(kJ mol^{-1})		
	(AD)	(AE)	(AF)
400	−42.33	−66.67	−74.04
600	−57.93	−74.50	−175.86
800	−72.69	−82.13	−277.03
1000	−86.63	−89.47	−376.49

between 400 K and 1000 K, because the ΔG_r value for the MnO reduction is higher than 100 kJ mol^{-1}.

The difficult reduction of MnO has the consequence that manganese carbides are not produced even under strongly reducing conditions in the temperature range 400—1000 K. On the other hand, MnO can be oxidized to Mn_3O_4 (which exhibits the spinel character) and further to Mn_2O_3. Under lower temperatures and strongly oxidizing conditions the oxidation proceeds to MnO_2.

Mn_3O_4 and Mn_2O_3 can be relatively easily reduced to MnO as shown by the values of reaction Gibbs energy ΔG_r for their reduction by CO, hydrogen, and CH_4. The corresponding reactions for Mn_3O_4 and Mn_2O_3 are listed below and the relevant ΔG_r data for Mn_3O_4 reactions are summarized in Table 12. The ΔG_r values for reduction of Mn_2O_3 are more negative than those calculated for the reduction of Mn_3O_4, *i.e.* Mn_2O_3 could be very easily reduced to MnO.

$$Mn_3O_4(s) + H_2(g) \longleftrightarrow 3MnO(s) + H_2O(g) \quad (AD)$$

$$Mn_3O_4(s) + CO(g) \longleftrightarrow 3MnO(s) + CO_2(g) \quad (AE)$$

$$4Mn_3O_4(s) + CH_4(g) \longleftrightarrow 12MnO(s) + CO_2(g) + 2H_2O(g) \quad (AF)$$

Table 13. Reaction Gibbs Energy, Equilibrium Constant, and Equilibrium Hydrogen Mole Fraction in the Gas Phase for the Reverse Reaction (AD)

T/K	ΔG_r/(kJ mol^{-1})	$K_r \cdot 10^6$	x_{H_2}/vol. %
400	42.33	2.8997	0.00029
600	57.93	8.8674	0.00089
800	72.69	17.611	0.00176
1000	86.63	29.303	0.00293

$$Mn_2O_3(s) + H_2(g) \longleftrightarrow 2MnO(s) + H_2O(g) \quad (AG)$$

$$Mn_2O_3(s) + CO(g) \longleftrightarrow 2MnO(s) + CO_2(g) \quad (AH)$$

$$4Mn_2O_3(s) + CH_4(g) \longleftrightarrow 8MnO(s) + CO_2(g) + 2H_2O(g) \quad (AI)$$

The reaction enthalpy values for the reactions (AD) and (AE) between the temperatures of 400—1000 K are approximately in the range from −10.3 kJ mol^{-1} to −18.88 kJ mol^{-1} and from −50.9 kJ mol^{-1} to −53.62 kJ mol^{-1}, respectively. Thus, the reduction of both Mn_3O_4 and Mn_2O_3 is thermodynamically favored. On the other hand, only Mn_3O_4 formation *via* the steam oxidation of MnO is thermodynamically allowed; however, the equilibrium conversion of water vapor is very low as shown in Table 13.

In order to increase the H_2 equilibrium mole fraction in the gas phase the activity of Mn_3O_4 should be lowered. One of the possible routes is the formation of stable spinel (*e.g.* similar to that of MgO [29]). However, this spinel should be more stable than the "manganese spinel" Mn_3O_4. Formation of Mn_3O_4 from MnO and Mn_2O_3 in the temperature range of 400—1000 K is characterized by the ΔG_r values between −28 kJ mol^{-1} and −38 kJ mol^{-1}. Therefore, support materials for MnO should be relatively nonreactive. Alumina is not a convenient support material (carrier) for the steam oxidation of MnO. At given reaction conditions, relatively stable spinel $MnAl_2O_4$ is formed with $\Delta G_r < -60$ kJ mol^{-1}. During the steam oxidation of MnO, the spinel $MnAl_2O_4$ has to be primarily decomposed, which requires chemical energy. Spinels like $NiO \cdot Mn_2O_3$ [30] and ferrites like $MnO \cdot Fe_2O_3$ [31] can modify the reduction and oxidation properties of the MnO—Mn_3O_4 and Ni—NiO systems by changing the activity of ferrite and spinel components. Practical application and improvement of such manganese compounds in redox cyclic processes is improbable or doubtful.

Under reducing conditions and at higher partial pressure of CO_2, MnO and Mn_3O_4 form relatively stable manganese carbonate $MnCO_3$

$$MnO(s) + CO_2(g) \longleftrightarrow MnCO_3(s) \quad (AJ)$$

Table 14. Reaction Gibbs Energy for the Formation of $MnCO_3$

T/K	ΔG_r/(kJ mol^{-1})		
	(AJ)	(AK)	(AL)
400	−40.347	−187.715	−163.374
500	−21.784	−135.955	−115.591
600	−3.417	−84.748	−68.184
700	14.745	−34.103	−21.176

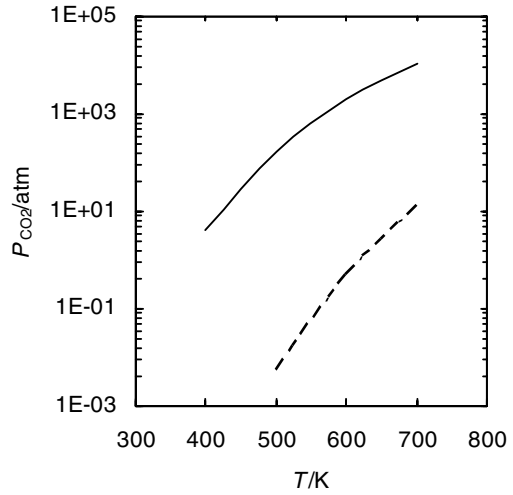

Fig. 5. Comparison of the equilibrium CO_2 pressure during the decomposition of $NiCO_3$ (solid line) and $MnCO_3$ (dashed line).

$$Mn_3O_4(s) + 2CO_2(g) + CO(g) \longleftrightarrow 3MnCO_3(s) \quad (AK)$$

$$Mn_3O_4(s) + 3CO_2(g) + H_2(g) \longleftrightarrow 3MnCO_3(s) + H_2O(g) \quad (AL)$$

ΔG_r values of the reactions leading to $MnCO_3$ formation are given in Table 14. The values of Gibbs energy of formation and enthalpy of formation for $MnCO_3$ are tabulated only up to a temperature of 700 K [17]. Comparing the respective equilibrium partial pressure of CO_2 one can conclude that within the temperature range of 400—700 K $MnCO_3$ is substantially more stable than $NiCO_3$ (Fig. 5).

Carburization Reactions, Carbon Deposition, and Metal Dusting

At strongly reducing conditions, in gaseous mixtures containing CO, CH_4, or higher hydrocarbons, elemental carbon can be formed, leading to carbon deposition, carburization, carbide formation, and metal dusting [32—36]. Butane was chosen to represent carburization behavior of higher hydrocarbons.

$$CO(g) + H_2(g) \longleftrightarrow C(s) + H_2O(g) \quad (AM)$$

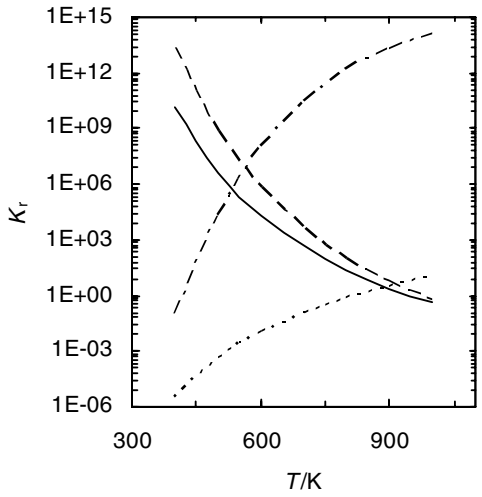

Fig. 6. Variation of the equilibrium constant of the reaction (AM) (solid line), (AN) (dashed line), (AO) (dotted line), and (AP) (dotted-dashed line) with temperature.

$$2CO(g) \longleftrightarrow C(s) + CO_2(g) \quad (AN)$$

$$CH_4(g) \longleftrightarrow C(s) + 2H_2(g) \quad (AO)$$

$$C_4H_{10}(g) \longleftrightarrow 4C(s) + 5H_2(g) \quad (AP)$$

Variation of the equilibrium constant of the abovementioned reactions with temperature (400—1000 K) is shown in Fig. 6.

The presence of higher hydrocarbons in the reducing gas contributes significantly to the carbon deposition. The formation of carbon by reactions (AM) and (AN) is enhanced at higher operating pressures, while the decomposition of hydrocarbons to hydrogen and carbon is suppressed. The presence of relatively high concentrations of water vapor generally reduces or even completely suppresses the carbon formation and deposition.

Metallic surfaces (*e.g.* Ni) or relevant carbide surfaces (Fe_3C) catalyze the deposition of carbon. On the other hand, at reducing conditions MnO inhibits carbon deposition. Compact surface layers of Cr_2O_3 protect metals such as Fe and Ni against carbon deposition [33, 36]. The catalytic activity of nickel catalysts for methane decomposition is strongly related to the crystalline size of the Ni particles [35]. Small crystallites (about 10 nm) exhibit high catalytic activity for the CH_4 decomposition and carbon deposition, whilst Ni crystallites above 24 nm are almost inactive in this reaction.

Hydrogen Production and Storage Potential

The maximum potential production capacity of hydrogen of the Fe—Fe_3O_4, Ni—NiO, and MnO—Mn_3O_4 systems is shown in Table 15. For comparison, also the equilibrium hydrogen concentration in

Table 15. Comparison of the Hydrogen Equilibrium Content in the Vapor Phase and the Maximum Capacity of Hydrogen Production in Terms of H_2/Me and H_2/Me_xO_y Mass Ratio for the 100 % Conversion of Water Vapor to Hydrogen Assuming the Redox Systems Fe—Fe_3O_4, Ni—NiO, and MnO—Mn_3O_4 at 600 K

Reaction	Form		Mass ratio · 10^2		x/vol. %
	Reduced	Oxidized	H_2/reduced form	H_2/oxidized form	
(R)	Fe	Fe_3O_4	4.77	3.45	94.86
(V)	Ni	NiO	3.41	2.68	0.236
Reverse (AD)	MnO	Mn_3O_4	0.94	0.87	0.00089

the gas phase is presented at 600 K for the chosen Me-Me_xO_y systems. The iron—magnetite redox pair exhibits the maximum potential productivity from the three mentioned systems applicable for hydrogen production (*e.g.* by syngas transformation) or for hydrogen storage. The system Ni—$NiAl_2O_4$ has substantially lower theoretical hydrogen capacity than the Ni—NiO system, but substantially higher equilibrium hydrogen concentration attainable. The system (Ni + 2Fe)—$NiFe_2O_4$ has slightly lower theoretical hydrogen production capacity than the Fe—Fe_3O_4 system, but higher than the Ni—NiO system. Reduction under milder reducing conditions is potential advantage of the system with nickel ferrite against the iron—magnetite system. However, the oxidation step, transforming Ni + 2Fe by steam oxidation to $NiFe_2O_4$, is from the thermodynamics point of view practically excluded.

Acknowledgements. This research was carried out within the European Commission's Research and Development Program.

REFERENCES

1. Messerschmitt, A., *Ger.* DE 266863 (1911).
2. Fraser, S. and Hacker, V., *Sponge Iron Process for Manned Space Exploration*, Final Project Report, Technical Officer: Dr. Tiziana Pipoli, Ariadna Contract No. 18461/04/NL/MV, 2005.
3. Hacker, V., Fankhauser, R., Faleschini, G., Fuchs, H., Friedrich, ,K., Muhr, M., and Kordeschet, K., *J. Power Sources 86*, 531 (2000).
4. Hacker, V., Faleschini, G., Fuchs, H., Fankhauser, R., Simader, G., Ghaemi, M., Spreitz, B., and Friedrichet, K., *J. Power Sources 71*, 226 (1998).
5. Lundberg, M., *Int. J. Hydrogen Energy 18*, 369 (1993).
6. Inoue, M., Hasegawa, N., Uehara, R., Gokon, N., Kaneko, H., and Tamaura, Y., *Sol. Energy 76*, 309 (2004).
7. Adanez, J., de Diego, L. F., Garcia-Labiano, F., Gayan, P., Abad, A., and Palacios, J. M., *Energy Fuels 18*, 371 (2004).
8. Son, S. R. and Kim, S. D., *Ind. Eng. Chem. Res. 45*, 2689 (2006).
9. Cao, Y. and Pan, W.-P., *Energy Fuels 20*, 1836 (2006).
10. Mattisson, T., Johansson, M., and Lyngfelt, A., *Fuel 85*, 736 (2006).
11. Hacker, V., *J. Power Sources 118*, 311 (2003).
12. Otsuka, K., Kaburagi, T., Yamada, C., and Takenaka, S., *J. Power Sources 122*, 111 (2003).
13. Takenaka, S., Sou, V. T. D., and Otsuka, K., *Energy Fuels 18*, 820 (2004).
14. Urasaki, K., Tanimoto, N., Hayashi, T., Sekine, Y., Kikuchi, E., and Matsukata, M., *Appl. Catal., A 228*, 143 (2005).
15. Hui, W., Takenaka, S., and Otsuka, K., *Int. J. Hydrogen Energy 31*, 1732 (2006).
16. Cho, P., Mattisson, T., and Lyngfelt, A., *Ind. Eng. Chem. Res. 44*, 668 (2005).
17. Barin, I. and Knacke, O., *Thermochemical Data of Pure Substances*, 3rd Edition. VCH, Weinheim, 1995.
18. Tseng, W. J., Hsu, C.-K., Chi, C.-C., and Teng, K.-H., *Mater. Lett. 52*, 313 (2002).
19. Kenfack, F. and Langbein, H., *Cryst. Res. Technol. 41*, 748 (2006).
20. Bučko, M. and Haberko, K., *J. Eur. Ceram. Soc.*, in press.
21. Bolt, P. H., Habraken, F. H. P. M., and Geus, J. W., *J. Solid State Chem. 135*, 59 (1998).
22. Twigg, M. V. and Richardson, J. T., *Appl. Catal., A 190*, 61 (2000).
23. Readman, J. E., Olafsen, A., Smith, J. B., and Blom, R., *Energy Fuels 20*, 1382 (2006).
24. Svoboda, K., Slowinski, G., Rogut, J., and Siewiorek, A., *17th International Congress of Chemical and Process Engineering CHISA*, Prague, 2006.
25. Villa, R., Cristiani, C., Groppi, G., Lietti, L., Forzatti, P., Cornaro, U., and Rossini, S., *J. Mol. Catal. A: Chem. 204*, 637 (2003).
26. Li, G. H., Hu, L. J., and Hill, J. M., *Appl. Catal., A 301*, 16 (2006).
27. Stobbe, E. R., de Boer, B. A., and Geus, J. W., *Catal. Today 47*, 161 (1999).
28. Terayama, K., Ikeda, M., and Taniguchi, M., *Trans. Jpn. Inst. Met. 24*, 24 (1983).
29. Malavasi, L., Ghigna, P., Chiodelli, G., Maggi,G., and Flor, G., *J. Solid State Chem. 166*, 171 (2002).
30. Christel, L., Pierre, A., and Abel, D. A. M. R., *Thermochim. Acta 306*, 51 (1997).
31. Guillemet-Fritsch, S., Navrotsky, A., Tailhades, P., Coradin, H., and Wang, M., *J. Solid State Chem. 178*, 106 (2005).
32. Jablonski, G. A., Geurts, F. W., Sacco, A., and Biederman, R. R., *Carbon 30*, 87 (1992).
33. Grabke, H. J. and Wolf, I., *Mater. Sci. Eng. 87*, 23 (1987).

34. Mallon, C. and Kendall, K., *J. Power Sources 145*, 154 (2005).
35. Li, Y., Zhang, B. C., Xie, X. W., Liu, J. L., Xu, Y. D., and Shen, W. J., *J. Catal. 238*, 412 (2006).
36. Zeng, Z. and Natesan, K., *Solid State Ionics 167*, 9 (2004).